Nanoscale

Dynamic Article Links ►

Cite this: DOI: 10.1039/c0xx00000x

www.rsc.org/xxxxxx

Paper

Investigation of Non-Segregation Graphene Growth on Ni *via* Isotope-Labeled Alcohol Catalytic Chemical Vapor Deposition

Pei Zhao,[a] Bo Hou,[a] Xiao Chen,[a] Sungjin Kim,[a] Shohei Chiashi,[a] Erik Einarsson[a,b] and Shigeo Maruyama*[a]

Received (in XXX, XXX) Xth XXXXXXXXX 20XX, Accepted Xth XXXXXXXXX 20XX
DOI: 10.1039/b000000x

Here we present CVD growth of graphene on Ni and investigate the growth mechanism using isotopically labeled ^{13}C-ethanol as the precursor. Results show that during low-pressure alcohol catalytic CVD (LP-ACCVD), a growth time of less than 30 s yields graphene films with high surface coverage (>80%). Moreover, when isotopically labeled ethanol precursors were sequentially introduced, Raman mapping revealed that both ^{12}C and ^{13}C graphene flakes exist. This shows that even at high temperature (~900 °C) the graphene flakes form independently, suggesting a different growth mechanism for ethanol-derived graphene on Ni from the segregation process for methane-derived graphene. We interpret this growth mechanism using a direct surface-adsorptive growth model in which small carbon fragments catalyzed from ethanol decomposition products first nucleate at metal step edges or grain boundaries to initiate graphene growth, and then expand over the entire metal surface.

1 Introduction

Graphene, a revolutionary material with atomic thickness, has been attracting extensive attention in nanoscience and technology.[1] Its many unique properties have made graphene one of the leading candidates for a wide range of applications in electronic devices, photovoltaics, batteries, nanocomposites, etc.[2] However, simple and controllable synthesis of large-scale graphene films still poses one of the major challenges towards the practical utilization of graphene to its full potential. Many physical or chemical approaches have been developed, including microcleavage of highly oriented pyrolytic graphite (HOPG),[3] epitaxial growth on silicon carbide,[4] chemical reduction of graphene oxide,[5] and chemical vapor deposition (CVD) of hydrocarbon gas precursors or solid carbon sources in the presence of metal substrates.[6-14] Among these methods, CVD has proven to be the most advantageous and inexpensive to obtain high-quality graphene films up to inch-scale.[15]

Various transition metals have been reported as catalytic substrates to grow graphene, such as Ni,[6, 7] Cu,[8] Co,[9] Ru,[10] Ir,[11] Pd,[12] and Pt.[13] However, the underlying mechanisms for CVD graphene growth on these substrates have yet to be totally clarified, especially for synthesis on Ni, the first-reported and one of the most widely used metal substrates. A widely accepted synthesis model is based on the high solubility of C in Ni at high temperature (~0.9 at.% at 900 °C). According to the model, C atoms supplied by the precursor dissolve into the bulk Ni, forming a stable single-phase Ni-C solution. As the substrate cools, a condensed "graphitic monolayer" forms first within a narrow temperature window of ~100 K. This is known as "segregation", and corresponds to a single-phase equilibrium with compositional heterogeneity. Single-layer graphene (SLG) is always formed during this step. As the Ni cools further, the phase-separation process of precipitation occurs for the remaining dissolved C atoms, forming additional layers or even graphite.[16] This model is supported by results from Auger spectroscopy and in situ scanning electron microscopy (SEM) on Ni foils that had been pre-doped with C atoms.[16-18] Li et al. [19] extended this model to the CVD process, and their work using carbon isotope labeling clearly confirmed the dissolution-segregation-precipitation mechanism for graphene growth on Ni when methane is used as the precursor. According to this model, an appropriate cooling rate and segregation temperature window are necessary to obtain high-quality SLG samples.

However, other growth mechanisms have also been proposed. For instance, Weatherup et al.[20] showed that at low temperature (~600 °C) uniform SLG formation can occur and be optimized by locally saturating only the catalyst surface with carbon. No segregation takes place during this process. Because the bulk Ni just acts as a mediating carbon sink in this model, the SLG growth can even be catalyzed on a thick Ni foil, which is usually considered a disadvantage in the dissolution-segregation model due to the difficulties in controlling the precipitation of the large amount of carbon dissolved in the foil. This model was proposed based on the experimental results using benzene and acetylene, which are more reactive than the methane precursor more commonly used for graphene growth.

The difference in the above growth models suggests that the CVD mechanism on Ni surface using various carbon sources has not been totally clarified. Moreover, for non-hydrocarbon precursors with low dissociation energies, their numerous decomposition products may lead to more complicated interfacial reactions, therefore it is of significant interest to explore the surface kinetics and mechanisms behind the conversion into well-formed graphene lattices.

In this work, we present CVD growth of few layer graphene films on Ni surface and investigate its mechanism using isotopically labeled ^{13}C-ethanol as the precursor. Results show that during low-pressure alcohol catalytic CVD (LP-ACCVD), a growth time of less than 30 s yields graphene films with high surface coverage (>80%). Moreover, when isotopic ethanol precursors are sequentially introduced, micro-Raman scanning maps reveal that both ^{12}C and ^{13}C graphene flakes co-exist, rather than forming a uniform mixture of ^{12}C and ^{13}C as predicted by the segregation model. This result shows that the sequentially introduced isotopic ethanol sources independently form graphene flakes on Ni, suggesting the growth mechanism for ethanol-derived graphene on Ni is not explained by the segregation or precipitation process. We interpret the graphene growth mechanism for ethanol using a non-segregation growth model, in which small carbon fragments from various decomposition products nucleate at metal step edges or grain boundaries to initialize graphene growth without a segregation or precipitation process. These flakes then expand to produce continuous graphene coverage over the entire metal surface with different layer numbers. This study will help clarify the growth mechanism of graphene on Ni from non-hydrocarbon precursors such as ethanol, and promote efforts to synthesize large-scale, high-quality graphene on non-copper metal substrates using various carbon sources.

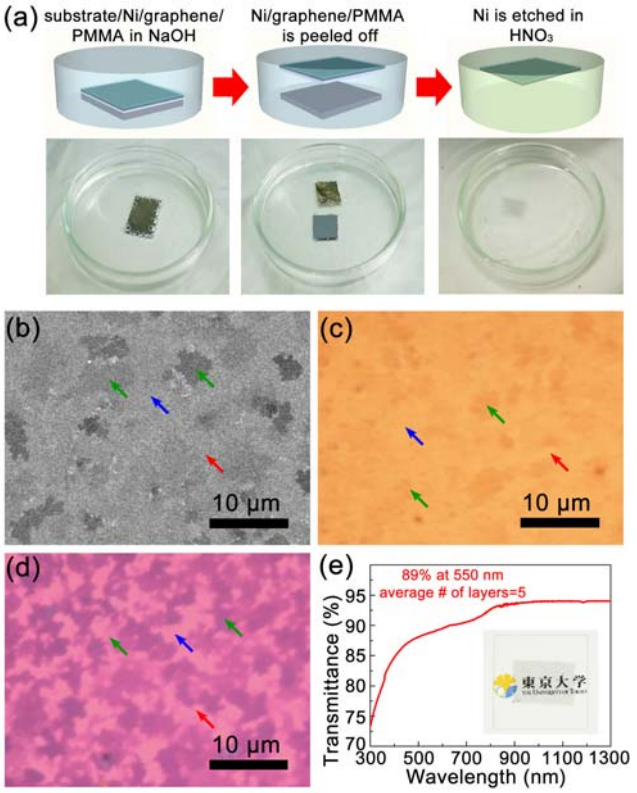

Fig. 1. (a) Transfer process of as-grown graphene films from Ni onto arbitrary substrates. (b) SEM image of as-grown ethanol-derived graphene on a 250-nm-thick Ni film. (c, d) Optical micrographs of a graphene film on Ni surface (c) and Si/SiO_2 substrate (d). Red, blue and green arrows in (b–d) indicate single-, bi- and few-layer graphene, respectively. (e) Transmittance of a transferred graphene film on a quartz substrate, measured from 300 to 1300 nm. Inset photograph shows the transparency of the transferred graphene sample.

2 Experimental Section

Synthesis. The ACCVD process was used for ethanol-derived graphene growth.[21] Polycrystalline Ni substrates were prepared by thermally evaporating a 250-nm-thick layer of Ni (99.99% pure) onto SiO_2 (50 nm)/Si wafers without any post-treatment of the surface. The substrates were then loaded into a hot-wall CVD quartz chamber (26 mm, i.d.), and heated to 900 °C under a flow of 3% H_2 in Ar to anneal the metal surface and remove oxide residues (pressure of ~40 kPa, flow rate of 300 sccm). After reaching the target temperature, the chamber was evacuated, 50 sccm of ethanol vapor was introduced for 2 min, and the substrate was then rapidly cooled to room temperature (~25 °C) at a rate of 10–20 °C·s^{-1}. For graphene growth from isotopic ethanol sources, an equivalent no-flow CVD process was adopted.[22] In this case, upon reaching the target temperature, 0.1 μL $^{12}C_2H_5OH$ (99%) was introduced into the chamber for 30 s or 60 s, followed by evacuating the ^{12}C residues and then introducing 0.1 μL $^{13}C_2H_5OH$ (99%, Cambridge Isotope Laboratory, Inc.) for another 30 s or 60 s. Finally the furnace was cooled to room temperature by the same rapid cooling process.

Transfer. As-grown graphene films were transferred to arbitrary substrates by the method shown in Fig. 1a. This is a modification of the method reported in Ref. (23). A layer of 4 wt.% poly(methyl methacrylate) (PMMA, MW=950k, dissolved in anisole) was spin-coated onto a graphene sample atop a Ni/SiO_2/Si substrate, and then baked at 150 °C for 30–60 min. The sample was then immersed in 1 M NaOH solution (80 °C) for 60 min, during which the PMMA/graphene/Ni layer slowly delaminated itself from the SiO_2/Si substrates due to the production of H_2 bubbles. An additional etching process using 10% HNO_3 at 80 °C isolated the graphene/PMMA film for transferring to arbitrary substrates. Finally, the PMMA protection layer was removed by hot acetone vapor (80 °C), followed by annealing the sample at 500 °C for 2–4 h under an atmosphere of Ar/H_2, which is necessary to remove PMMA residues and improve the graphene-substrate adhesion.

Characterization. Characterization of as-grown and transferred graphene samples consisted of scanning electron microscopy (SEM; S-4800, Hitachi Co. Ltd.), ultraviolet-visible-near infrared (UV-vis-NIR) spectroscopy (UV-3600, Shimadzu Co. Ltd.), and micro-Raman spectroscopy (RENISHAW inVia Reflex/StreamLine system, Shimadzu Co. Ltd.; and Raman-11 system, Nanophoton Co. Ltd.).

3 Results and discussion

CVD growth of graphene on Ni from ethanol

Most CVD growth of graphene on Ni uses methane as the

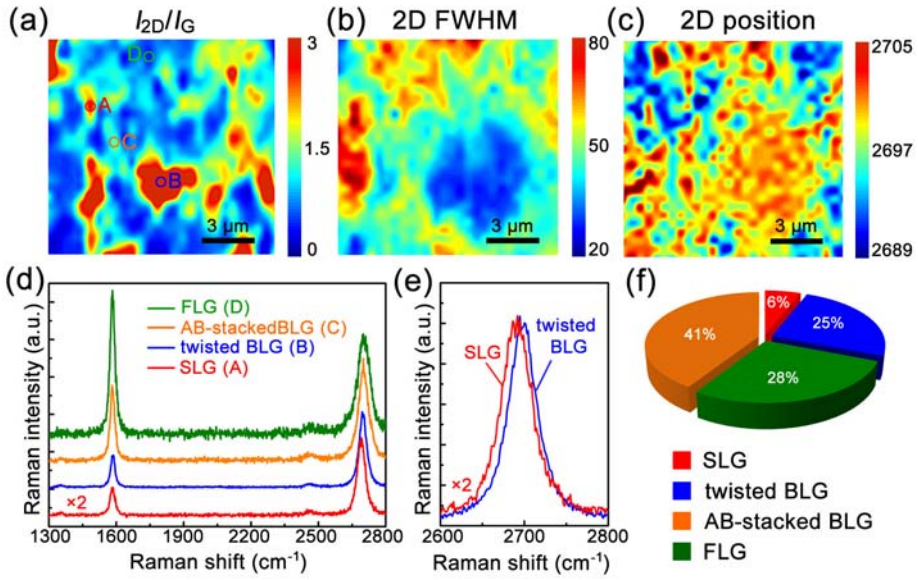

Fig. 2. (a–c) High-definition (0.6 μm resolution) scanning Raman maps of ethanol-derived graphene transferred onto a Si/SiO_2 substrate showing (a) I_{2D}/I_G, (b) 2D-band FWHM, and (c) 2D-band peak position. (d) Raman spectra of SLG, twisted BLG, AB-stacked BLG, and FLG obtained from corresponding positions A, B, C and D in (a). (e) Comparison of the Raman 2D-band peaks of SLG (red) and twisted BLG (blue). An upshift of ~9 cm^{-1} is observed for the 2D-band peak of twisted BLG. (f) Coverage statistics of SLG, twisted BLG, AB-stacked BLG and FLG, evaluated from the Raman spectra in (a–c).

hydrocarbon precursor. This has been reported to enable reproducible synthesis of graphene with some control over the number of layers.[6, 7] To increase the accommodation factor and catalytic reactivity of methane molecules on the Ni surface, ambient pressure CVD (AP-CVD) is usually adopted,[6, 7] but medium pressure CVD has also been reported.[24] Moreover, a high concentration of hydrogen is a necessity during growth to control the graphene formation rate by etching the formed carbon layers. In this case, caution needs to be taken when methane and hydrogen are involved at high temperature and pressure. Efforts toward graphene growth using non-methane precursors of benzene and acetylene have also been made under ultralow pressure CVD conditions.[20, 25]

Ethanol, a non-hydrocarbon precursor, has proven to be a low-cost, clean carbon source well suited for the synthesis of single-walled carbon nanotubes (SWNTs) with high purity and yield.[21] The oxygen in ethanol improves the quality of SWNTs by reacting with any amorphous carbon produced during synthesis. Moreover, ethanol offers selectivity in forming only single-walled carbon nanotubes.[21] In this sense, we suspect ethanol may also be advantageous when employed for graphene synthesis.

Fig. 1a shows the transfer process of an ethanol-derived graphene sample from Ni onto an arbitrary substrate.[23] A representative SEM image of graphene grown on a Ni (250 nm)/SiO_2 (50 nm)/Si substrate is shown in Fig. 1b. The clear difference in contrast shows graphene flakes with different layer numbers, with darker areas corresponding to more layers. Fig. 1c,d show optical microscopy (OM) images before and after the transfer of a graphene film from a Ni surface to a Si substrate with a 300-nm-thick oxide layer, respectively. After transfer, the color contrast between graphene flakes with different layer numbers becomes more visible. The red, blue and green arrows in Fig. 1b–d indicate areas of single-, bi- and few-layer graphene, respectively. We also measured the optical transmittance of an ethanol-derived graphene film from 300 nm to 1300 nm after transferring onto a quartz slide. The sample shows a transmittance of ~89% at 550 nm (Fig. 1e), corresponding to an average number of layers of 4 to 5 (the absorbance of one graphene layer is ~2.3%).[26] This corresponds to 2–6 fewer layers than reported for large-scale graphene obtained from methane on Ni (T=76.3% without UV treatment, or 83.7% after 6 h UV treatment).[7] The size of our graphene films is limited only by the surface area of the metal film and by the CVD chamber size. A photograph of as-grown graphene on Ni with size of 17×17 mm^2 is shown in Fig. S1 in the Electronic Supplementary Information (ESI).

Raman investigation of layer number

The uniformity of ethanol-derived graphene films and their spatial distribution of layer numbers were confirmed by high-definition Raman spectroscopy. Raman maps of a graphene film transferred onto a Si/SiO_2 substrate were obtained by collecting 27×28=756 Raman spectra over an area of ~250 μm^2, with a spatial resolution of 0.6 μm. Fig. 2a,b show contour maps of the intensity ratio of the 2D-band (2650–2750 cm^{-1}) to the G-band (1550–1610 cm^{-1}), i.e., I_{2D}/I_G, and the full-width-at-half-maximum (FWHM) of the 2D-band, respectively. Approximately 31% of collected Raman spectra feature an I_{2D}/I_G greater than 1.4 and a symmetric 2D-band with a FWHM smaller than 45 cm^{-1}, which is conventionally considered to be the Raman fingerprint of SLG. Bi-layer graphene (BLG), with an I_{2D}/I_G between 0.7 and 1.4 and a 2D-band FWHM between 45 and 60 cm^{-1}, has a coverage of 41% of the measured area.[27] The remaining 28% of Raman spectra show characteristics typical of few-layer graphene (FLG, layer number ≥ 3), such as a

low I_{2D}/I_G ratio and a broad, asymmetric 2D-band peak. Typical Raman spectra obtained from the corresponding locations A, B, C and D in Fig. 2a are shown in Fig. 2d. We note that in these spectra the intensity of the D-band (~1350 cm^{-1}), which indicates the presence of structural defects, is negligible (I_G/I_D > 20) even after the transfer process. This suggests ethanol-derived graphene films are overall very high quality and the transfer procedures is essentially non-destructive. Low-definition (10 μm spatial resolution) Raman contour maps show similar spatial distributions of SLG, BLG and FLG over a larger scanning area of ~8000 μm^2, as shown in Fig. S2 in ESI.

The above discussion on the number of graphene layers and their relation with Raman spectral features are based on the assumption that the BLG areas have the most energetically preferred Bernal (AB) stacking configuration, in which a carbon atom in one layer is located at the center of the hexagon of the neighboring layer. The strong interlayer coupling in Bernal stacking causes the linear π-electron dispersion near the K-point to split into two parabolic branches, leading to four double-resonance Raman scattering processes.[28] If the two SLG layers in BLG are twisted with an angle between 0º and 60°, a moiré pattern occurs and the interlayer coupling becomes considerably weaker.[29] Twisted BLG with moiré patterns have been widely observed for CVD graphene grown on transition metals.[10, 30-32] The weak coupling between two SLG layers in twisted BLG eliminates the interlayer double-resonance processes. This makes the 2D-band of a twisted BLG very narrow and – similar to the Raman spectrum of SLG – can be fitted by a single symmetric Lorenzian lineshape. However, due to the reduction of the Fermi velocity in twisted BLG, there is an upshift of ~10 cm^{-1} for the 2D-band of twisted BLG compared to SLG.[33]

To distinguish the twisted BLG areas from real SLG ones, we plot in Fig. 2c a contour map showing the center position of the Raman 2D feature. The scanned area is the same as in Fig. 2a,b. For all Raman spectra collected in this area that display SLG features, ~80% exhibit a 2D-band centered at ~2700 cm^{-1}, which corresponds to a 7–11 cm^{-1} upshift compared with the remaining 20% of Raman spectra. We note that no shift was observed for the G-band peaks, suggesting that effects due to strain and doping can be excluded. Therefore, we conclude that the 80% of conventional "SLG" that show upshifts in their 2D-band are actually twisted BLG. Fig. 2d shows a representative Raman spectrum corresponding to spot B in Fig. 2a, which has features of SLG analogous to those for spot A, but with an apparent upshift of ~9 cm^{-1} in its 2D-band.

Taking into consideration the above discussion, the spatial distribution of SLG, twisted BLG, AB-stacked BLG and FLG in the graphene films grown from ACCVD is shown in Fig. 2f. The coverage statistics show that 28% of collected spectra in the scanned area are from FLG, 41% are from AB-stacked BLG, 25% are from twisted BLG and 6% are from true SLG. The coverage of SLG and AB-stacked BLG (~47%) is higher than the previously reported value (~10%) for epitaxial graphene segregated from C-doped Ni substrates.[34]

CVD time dependence of graphene growth

It is of particular interest to explore the growth mechanism of graphene on Ni surface using precursors other than methane. To understand the formation process of graphene from ethanol, we first examined the effect of CVD growth time. OM and SEM images of the Ni surface after H_2 annealing (prior to ethanol exposure), after 30 s ethanol exposure, and after 5 min ethanol exposure are shown in Fig. 3. Compared with the bare Ni surface obtained after H_2 annealing, 30 s of ethanol exposure leads to graphene growth with considerable coverage of the metal surface (> 80%). Uncovered areas are indicated by red arrows in Fig. 3e. The SEM image in Fig. 1c and Raman imaging maps in Fig. 2a–c show that a growth time of 2 min achieves 100% graphene coverage of the Ni surface. When the CVD growth time was further prolonged to 5 minutes, the coverage of dark areas composed of multi-layer graphene significantly increases, as shown in Fig. 3c,f. Transparency measurements of these films show consistent results, in which longer exposure to ethanol produced graphene with reduced transparency (i.e., more layers). For instance, the graphene film grown for 5 min has a transmittance of ~76% (Fig. S3 in ESI), corresponding to an average layer number of ~10–11.

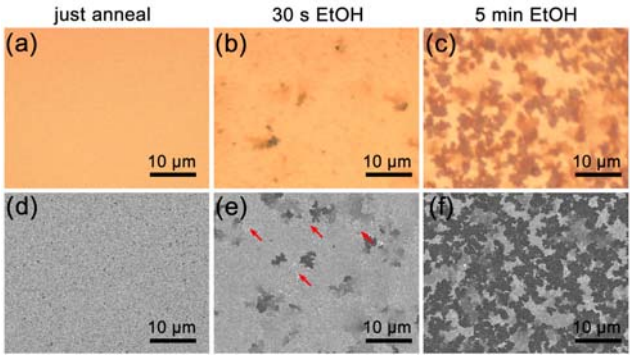

Fig. 3. Optical (a–c) and SEM (d–f) images of as-grown graphene on Ni surface with different exposure time to ethanol. (a, d) After H_2 annealing but prior to growth; (b, e) after 30 s exposure to ethanol; (c, f) after 5 min exposure to ethanol. Red arrows in (e) indicate areas of bare Ni uncovered by graphene.

Sequential growth of graphene with isotope-labeled ethanol

To further investigate the growth mechanism of graphene from ethanol, we adopted isotope labeling to track the carbon atoms during the CVD process. Sequentially introduced ethanol precursors containing different carbon isotopes, i.e. ^{12}C or ^{13}C, was used for equivalent-time no-flow CVD graphene growth. A CVD trial using 10 seconds $^{12}C_2H_5OH$ followed by 10 seconds $^{13}C_2H_5OH$ was initially performed. As shown in Fig. S4 in ESI, the Raman spectrum measured from this as-grown graphene sample shows the presence of both isotopically pure ^{12}C- and ^{13}C-graphene, as evidenced by corresponding Raman G peaks located at ~1580 cm^{-1} and ~1525 cm^{-1}, respectively. The rapid formation of graphene films within such a short reaction time confirms the efficient conversion of ethanol molecules into graphene. More importantly, the two independent ^{12}C and ^{13}C G peaks is contrary to the result reported by Li et al., in which sequentially introduced $^{13}CH_4$ and $^{12}CH_4$ resulted in a single G peak located at ~1553 cm^{-1}, indicating graphene comprised of a mixture of ^{12}C and ^{13}C.[19] The dissolution/segregation model was hence clearly confirmed for CVD growth of graphene from methane,[19] but the co-existence of both ^{12}C and ^{13}C G-band peaks shown here clearly indicates that ^{12}C and ^{13}C isotopes have

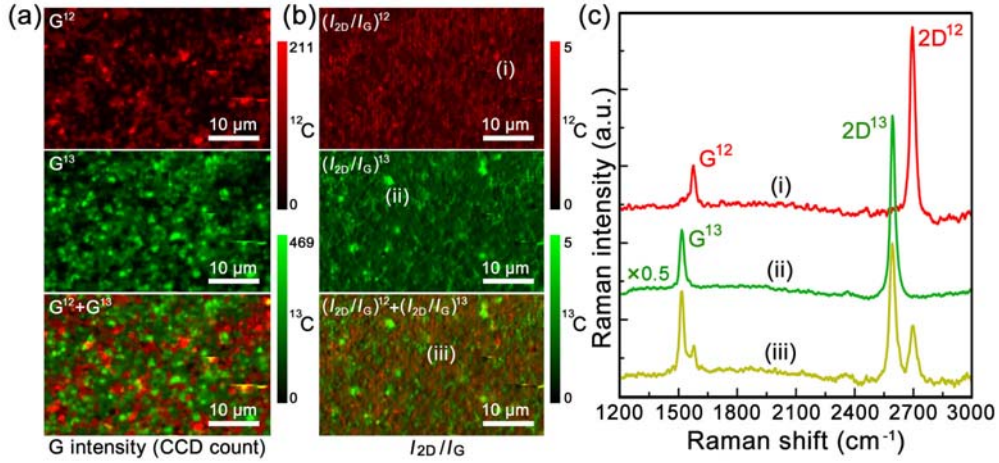

Fig. 4. High-definition scanning Raman maps of an ethanol-derived graphene film grown from 30 s $^{12}C_2H_5OH$ and sequential 30 s $^{13}C_2H_5OH$ and then transferred onto a Si/SiO_2 substrate. The ^{12}C and ^{13}C areas are shown in red and green, respectively. (a) From top to bottom: integrated Raman intensity maps of G^{12} (1550-1610 cm^{-1}), G^{13} (1500-1560 cm^{-1}), and G^{12}+G^{13} (1500-1610 cm^{-1}). (b) From top to bottom: integrated Raman maps of $^{12}(I_{2D}/I_G)$, $^{13}(I_{2D}/I_G)$, and $^{12}(I_{2D}/I_G)$+$^{13}(I_{2D}/I_G)$. (c) Raman spectra measured from different spots (i)–(iii) in (b) of this sample show features of ^{12}C or/and ^{13}C graphene.

undergone independent reaction processes to form graphene. This strongly suggests that graphene synthesis on Ni from ethanol is different from the dissolution/ segregation model.

To obtain a higher coverage of graphene and clearer Raman spectral features, we increased the reaction time of each isotopic ethanol precursor to 30 s, and the Raman imaging results of a graphene film transferred onto Si/SiO_2 are shown in Fig. 4. These Raman maps were obtained using a laser illumination scanning system with a spatial resolution of 350 nm. Fig. 4a shows contour maps of G-peak intensities for ^{12}C areas (G^{12}, 1560–1610 cm^{-1}), 13C areas (G^{13}, 1500–1560 cm^{-1}), and their overlaps (G^{12}+G^{13}, 1500–1610 cm^{-1}). Higher G-band peak intensities indicate more in-plane graphitic vibrations and hence more graphene layers. Raman G-band intensities from both ^{12}C and ^{13}C were observed on Ni, showing the existence of graphene flakes formed by these two isotopes. Moreover, as shown in the lower panel of Fig. 4a, it is clear that the ^{12}C areas (red) and ^{13}C areas (green) are complementary (no overlap of red and green, except for some very small areas shown in yellow). These preferential formations cannot be interpreted by the enhanced precipitation of carbon atoms at the step edges or grain boundaries, because the precipitation of dissolved ^{12}C and ^{13}C atoms would lead to FLG with a uniform mixture of these isotopes, and thus would show a single Raman G-band feature centered at ~1555 cm^{-1}. The distributions of ^{12}C- and ^{13}C-graphene are plotted in Fig. 4b, characterized by their I_{2D}/I_G. However, no large graphene flakes were observed for either ^{12}C- or ^{13}C-graphene when the exposure time was only 30 s for each isotopic ethanol. Typical Raman spectra of the isotopic graphene taken from spots (i)–(iii) in Fig. 4b are shown in Fig. 4c. It is noteworthy that in this graphene sample, both isolated ^{12}C and ^{13}C graphene can be observed without signals from the other isotope, as shown in spectra (i) and (ii), suggesting that the graphene flakes initially form independently, then expand out across the surface.

The exposure time of each isotopic ethanol precursor was further increased to 60 s and the corresponding Raman imaging results of the resulting graphene film (transferred on Si/SiO_2) are shown in Fig. 5. However, unlike the results in Fig. 4a, both G^{12} and G^{13} peaks shown in Fig. 5a have maximum intensities at approximately the same locations rather than in complementary patterns, as indicated by the white arrows in Fig. 5a. Large flakes were observed for both ^{12}C- and ^{13}C-graphene in this sample, as shown by the clear bright areas in Fig. 5b.

Typical Raman spectra measured from this isotopic graphene are shown in Fig. 5c, and are decomposed into their ^{12}C and ^{13}C components by Lorentzian lineshapes. More information about these ^{12}C- and ^{13}C-graphene flakes can be derived from these Raman maps and spectra. Firstly, as discussed above, with longer growth time the SLG, BLG, and FLG flakes are found at approximately the same areas for both ^{12}C- and ^{13}C ethanol-derived graphene films. Overlaps of ^{12}C- and ^{13}C-graphene films show that the Ni surface morphology probably plays the same role in graphene formation for both precursors. Secondly, graphene samples with different layer numbers were observed for both ^{12}C- and ^{13}C-graphene, showing that when isotopic ethanol is employed, the Ni surface does not have any selectivity or preference for graphene growth with a certain number of layers (i.e., is not self-limiting). Thirdly and more importantly, Raman G-band signals from ^{12}C-SLG, BLG and FLG could be observed without ^{13}C-graphene signals, as shown in spectra (i) and (ii) in Fig. 5c, but G-band signals from ^{13}C-graphene flakes were always observed with ^{12}C G-band signals [for instance, spectra (iii)–(vi) in Fig. 5c]. This indicates that after 60 s ^{12}C ethanol exposure followed by 60 s ^{13}C ethanol exposure, the Ni surface is always covered by ^{12}C-graphene but not always by ^{13}C-graphene, suggesting that the firstly-introduced 60 s of ^{12}C ethanol was converted into graphene with more extensive coverage than the secondly-introduced 60 s of ^{13}C ethanol. We attribute this to the reduction of the ^{13}C flux through the boundaries or defect sites of the formed ^{12}C-graphene layers,[20] which nucleates and forms additional layers when it is in contact with the Ni surface.

Raman spectra with different G-peak positions were also occasionally observed. Fig. 6a and 6b show contour maps of the

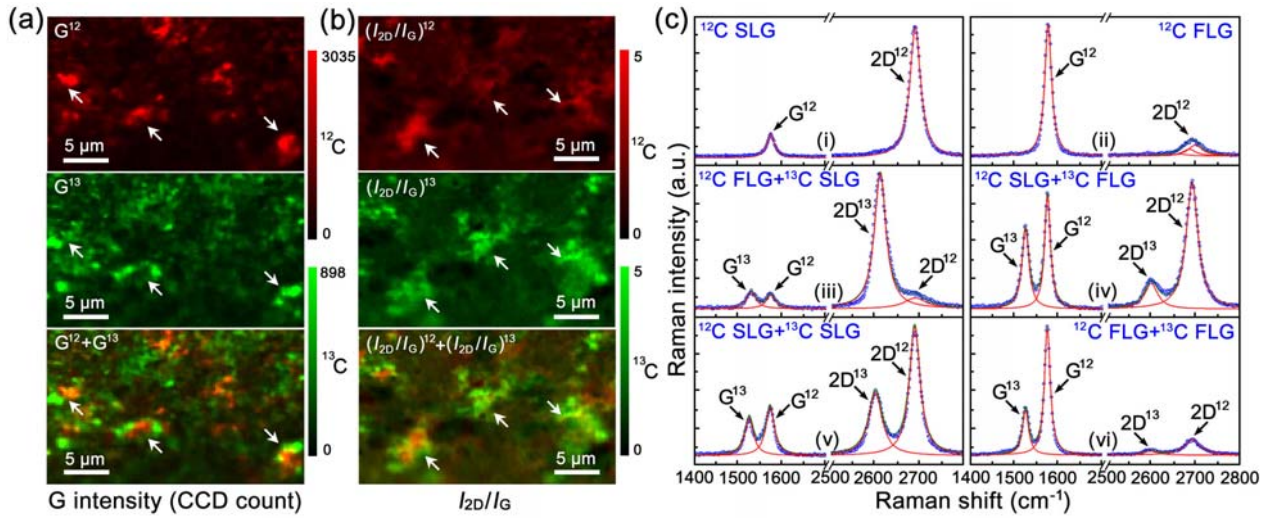

Fig. 5. High-definition Raman scanning images of a graphene film grown from 60 s exposure to $^{12}C_2H_5OH$ followed by 60 s $^{13}C_2H_5OH$. ^{12}C and ^{13}C areas are highlighted in red and green, respectively. (a) From top to bottom: integrated Raman intensity maps of G^{12}, G^{13}, and $G^{12}+G^{13}$. (b) From top to bottom: integrated Raman maps of $(I_{2D}/I_G)^{12}$, $(I_{2D}/I_G)^{13}$, and $(I_{2D}/I_G)^{12}+(I_{2D}/I_G)^{13}$. Arrows in (a) [or (b)] show areas with high G-band intensities (or I_{2D}/I_G) of ^{12}C and ^{13}C are preferentially overlapped. (c) Raman spectra measured from different spots of this sample show features of isotopic graphene consist of different layer numbers. Spots (i)–(vi) are shown in Fig. S5 in ESI.

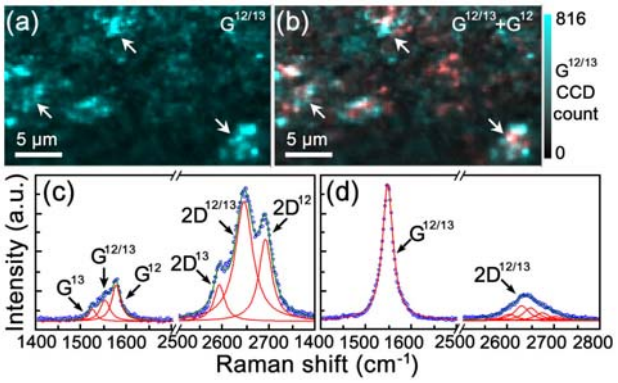

Fig. 6. (a) Spatial distribution of graphene flakes with G-band peak position at ~1550 cm^{-1} ($G^{12/13}$); (b) an overlapped contour map of $G^{12/13}$ with G^{12}; (c) a Raman spectrum measured from a tri-layer graphene area. The three layers are an overlap of ^{12}C-, ^{13}C- and $^{12}C/^{13}C$ mixed SLG; (d) a Raman spectrum measured from another tri-layer graphene area, all the three layers of which are formed by a uniform mixture of ^{12}C and ^{13}C.

G-band peaks located at ~1550 cm^{-1} ($G^{12/13}$) as well as their overlap with G^{12}, for the same isotopic graphene sample shown in Fig. 5. Interestingly, the high intensities of $G^{12/13}$ also occur at approximately the same areas as G^{12} and G^{13}, as indicated by white arrows. These spectra were observed either together with ^{12}C- and/or ^{13}C-graphene signals (Fig. 6c), or independent of peaks from ^{12}C- and ^{13}C-graphene (Fig. 6d).

Non-segregation growth of graphene on Ni from ethanol

The scanning Raman maps in Fig. 4 show that the growth mechanism for graphene formation on Ni surface from ethanol at high temperature is different from the widely accepted model of dissolution and segregation. Furthermore, Raman maps collected from the same isotopic graphene sample in Fig. 5 and Fig. 6 prove that two distinct mechanisms exist. When sequentially introduced ^{12}C- and ^{13}C-ethanol is used, graphene flakes consisting of ^{12}C and ^{13}C can be formed independently by one mechanism, whereas the other results in isotopically mixed graphene. The latter mechanism can be interpreted as a dissolution/segregation process similar to that of methane-derived graphene formation,19 or precipitation from a locally saturated Ni surface with dissolved carbon species.20 However, during CVD this segregation/precipitation process has a minor contribution to graphene formation from ethanol.

As for the former mechanism, which happens on Ni surface during the formation of graphene from ethanol, it is significant to investigate the scanning Raman maps shown in Fig. 4a in more detail. Although different from the well-distributed "ring" patterns when grown on copper,[19, 35] the G-band intensities of ^{12}C- and ^{13}C-graphene present a clear complementary pattern to cover the Ni surface, with few overlapped areas. This shows that the isotopic ethanol precursors are able to form graphene flakes independently on Ni surface in a non-segregation process.

The defect sites on Ni surface such as step edges and/or grain boundaries are also crucial in not only the growth mechanism but also the morphology of the formed graphene. For instance, Fig. 6 shows that high intensities of $G^{12/13}$ preferentially occur together at the same areas as G^{12} and G^{13}. We have assigned $G^{12/13}$ to the signal from graphene formed by the segregation process, in which the metal always results in enhanced precipitation of carbon atoms. It is also reasonable that these step edges and/or grain boundaries are enhanced catalysts to help independently form FLG flakes by ^{12}C and ^{13}C atoms. The existence and enhanced catalysis of the defect sites on Ni surface, as well as their ability to dissolve carbon species, help explains the varied distribution of SLG, BLG and FLG over the Ni surface.

On the basis of the above results and discussion, we propose a non-segregation growth model to interpret the graphene formation on Ni surface from ethanol at high temperature. In this process, various products of ethanol decomposition are partially

catalyzed by Ni and form small carbon fragments on the surface. Due to the fast surface saturation of Ni by the reactive carbon or buffering effects from the oxygen-containing decomposition products,[36, 37] these small carbon fragments nucleate and initiate graphene growth instead of being dissolved into the bulk Ni. The nucleated carbon chains or hexagonal lattices rapidly expand to form SLG flakes. This rapid expansion of SLG forms a thermally stable equilibrium with the Ni system at high temperature, analogous to the "segregation" state of the Ni-C system. Neighboring graphene flakes initialized from different step edges or grain boundaries coalesce to form continuous graphene films, covering the whole Ni surface. Extended growth time results in the formation of additional graphene layers when the carbon flux goes through the formed layers and in contact with the Ni surface.[20, 38, 39]

This model also better interprets the early work by Miyata et al. in which they reported a bubbled ethanol source can be used as a precursor for CVD growth of graphene on Ni foil (5 μm thick),[40] because the formation of graphene from ethanol on Ni surface is less dependent on the thickness of the metal.

4 Conclusions

Growth of graphene films on Ni substrates has been achieved by a low-pressure CVD method using ethanol vapor as the carbon precursor. CVD trials with extended growth times show that both the coverage and layer number of ethanol-derived graphene increase with prolonged growth time. Isotope-labeling experiments using $^{12}C_2H_5OH$ and $^{13}C_2H_5OH$ prove that graphene growth from ethanol occurs in a flake-by-flake fashion, rather than by a carbon dissolution and segregation process. This is evidenced by the presence of two coexisting Raman G-band peaks corresponding to independent ^{12}C- and ^{13}C-graphene regions, as opposed to the single-peak G-band feature exhibited by graphene consisting of mixed methane isotopes. Based on these results we propose a non-segregation model in which small carbon fragments catalyzed from ethanol first nucleate at the Ni surface, followed by expansion of the graphene layers. This mechanism dominates graphene growth on Ni surface from ethanol, while the dissolution/segregation process that governs graphene growth from methane only plays a minor role. The non-segregation mechanism described here can help further understand the formation of graphene on metal substrates using different CVD precursors especially more reactive non-hydrocarbons, and develop more controllable and inexpensive approaches for synthesizing large-scale uniform SLG or BLG films.

Acknowledgments

We thank Dr. Seiji Takeuchi from Shimadzu Co., Ltd. and Dr. Naoyoshi Kubota from Nanophoton Co. Ltd. for high-definition Raman imaging measurements. Part of this work was financially supported by Grants-in-Aid for Scientific Research (22226006, 23760179 and 23760180), and the Global COE Program "Global Center for Excellence for Mechanical Systems Innovation".

Notes and references

[a] *Department of Mechanical Engineering, The University of Tokyo, 7-3-1 Hongo, Bunkyo-ku, Tokyo 113-8656, Japan. Fax: +81-3-5800-6983; Tel: +81-3-5841-6421; Email: maruyama@photon.t.u-tokyo.ac.jp*
[b] *Global Center of Excellence for Mechanical Systems Innovation, The University of Tokyo, 7-3-1 Hongo, Bunkyo-ku, Tokyo 113-8656, Japan*

† Electronic Supplementary Information (ESI) available: Additional Raman imaging maps from as-grown (isotopic) graphene samples, as well as AFM images of Ni surfaces before and after H_2 annealing. See DOI: 10.1039/b000000x/

1. K. S. Novoselov, A. K. Geim, S. V. Morozov, D. Jiang, Y. Zhang, S. V. Dubonos, I. V. Grigorieva and A. A. Firsov, *Science*, 2004, **306**, 666-669.
2. A. K. Geim and K. S. Novoselov, *Nature Materials*, 2007, **6**, 183-191.
3. K. S. Novoselov, D. Jiang, F. Schedin, T. J. Booth, V. V. Khotkevich, S. V. Morozov and A. K. Geim, *Proc. Nat. Acad. Sci. USA*, 2005, **102**, 10451-10453.
4. C. Berger, Z. M. Song, X. B. Li, X. S. Wu, N. Brown, C. Naud, D. Mayou, T. B. Li, J. Hass, A. N. Marchenkov, E. H. Conrad, P. N. First and W. A. de Heer, *Science*, 2006, **312**, 1191-1196.
5. S. Stankovich, D. A. Dikin, R. D. Piner, K. A. Kohlhaas, A. Kleinhammes, Y. Jia, Y. Wu, S. T. Nguyen and R. S. Ruoff, *Carbon*, 2007, **45**, 1558-1565.
6. A. Reina, X. T. Jia, J. Ho, D. Nezich, H. B. Son, V. Bulovic, M. S. Dresselhaus and J. Kong, *Nano Lett.*, 2009, **9**, 30-35.
7. K. S. Kim, Y. Zhao, H. Jang, S. Y. Lee, J. M. Kim, K. S. Kim, J. H. Ahn, P. Kim, J. Y. Choi and B. H. Hong, *Nature*, 2009, **457**, 706-710.
8. X. S. Li, W. W. Cai, J. H. An, S. Kim, J. Nah, D. X. Yang, R. Piner, A. Velamakanni, I. Jung, E. Tutuc, S. K. Banerjee, L. Colombo and R. S. Ruoff, *Science*, 2009, **324**, 1312-1314.
9. A. Varykhalov and O. Rader, *Phys. Rev. B*, 2009, **80**, 035437.
10. P. W. Sutter, J. I. Flege and E. A. Sutter, *Nat. Mater.*, 2008, **7**, 406-411.
11. J. Coraux, A. T. N'Diaye, C. Busse and T. Michely, *Nano Lett.*, 2008, **8**, 565-570.
12. Y. Murata, E. Starodub, B. B. Kappes, C. V. Ciobanu, N. C. Bartelt, K. F. McCarty and S. Kodambaka, *Appl. Phys. Lett.*, 2010, **97**, 143114.
13. L. B. Gao, W. C. Ren, H. L. Xu, L. Jin, Z. X. Wang, T. Ma, L.-P. Ma, Z. Y. Zhang, Q. Fu, L.-M. Peng, X. H. Bao and H.-M. Cheng, *Nat. Commun.*, 2012, **3**, 7.
14. Z. Z. Sun, Z. Yan, J. Yao, E. Beitler, Y. Zhu and J. M. Tour, *Nature*, 2010, **468**, 549-552.
15. S. Bae, H. Kim, Y. Lee, X. F. Xu, J. S. Park, Y. Zheng, J. Balakrishnan, T. Lei, H. R. Kim, Y. I. Song, Y. J. Kim, K. S. Kim, B. Ozyilmaz, J. H. Ahn, B. H. Hong and S. Iijima, *Nat. Nanotechnol.*, 2010, **5**, 574-578.
16. J. C. Shelton, H. R. Patil and J. M. Blakely, *Surf. Sci.*, 1974, **43**, 493-520.
17. M. Eizenberg and J. M. Blakely, *Surface Science*, 1979, **82**, 228-236.
18. K. Takahashi, K. Yamada, H. Kato, H. Hibino and Y. Homma, *Surf. Sci.*, 2012, **606**, 728-732.
19. X. S. Li, W. W. Cai, L. Colombo and R. S. Ruoff, *Nano Lett.*, 2009, **9**, 4268-4272.
20. R. S. Weatherup, B. Dlubak and S. Hofmann, *ACS Nano*, 2012, **6**, 9996-10003.

21. S. Maruyama, R. Kojima, Y. Miyauchi, S. Chiashi and M. Kohno, *Chem. Phys. Lett.*, 2002, **360**, 229-234.
22. R. Xiang, Z. Zhang, K. Ogura, J. Okawa, E. Einarsson, Y. Miyauchi, J. Shiomi and S. Maruyama, *Jpn. J. Appl. Phys.*, 2008, **47**, 1971-1974.
23. L. Y. Jiao, B. Fan, X. J. Xian, Z. Y. Wu, J. Zhang and Z. F. Liu, *J. Am. Chem. Soc.*, 2008, **130**, 12612-12613.
24. L. Huang, Q. H. Chang, G. L. Guo, Y. Liu, Y. Q. Xie, T. Wang, B. Ling and H. F. Yang, *Carbon*, 2012, **50**, 6.
25. S. Entani, Y. Matsumoto, M. Ohtomo, P. V. Avramov, H. Naramoto and S. Sakai, *J. Appl. Phys.*, 2012, **111**, 064324.
26. R. R. Nair, P. Blake, A. N. Grigorenko, K. S. Novoselov, T. J. Booth, T. Stauber, N. M. R. Peres and A. K. Geim, *Science*, 2008, **320**, 1308-1308.
27. Z. W. Peng, Z. Yan, Z. Z. Sun and J. M. Tour, *ACS Nano*, 2011, **5**, 8241-8247.
28. L. M. Malard, J. Nilsson, D. C. Elias, J. C. Brant, F. Plentz, E. S. Alves, A. H. Castro and M. A. Pimenta, *Phys. Rev. B*, 2007, **76**, 201401(R).
29. A. H. MacDonald and R. Bistritzer, *Nature*, 2011, **475**, 182-182.
30. Z. Q. Luo, T. Yu, J. Z. Shang, Y. Y. Wang, S. Lim, L. Liu, G. G. Gurzadyan, Z. X. Shen and J. Y. Lin, *Adv. Func. Mater.*, 2011, **21**, 911-917.
31. A. Reina, S. Thiele, X. T. Jia, S. Bhaviripudi, M. S. Dresselhaus, J. A. Schaefer and J. Kong, *Nano Res.*, 2009, **2**, 509-516.
32. A. T. N'Diaye, J. Coraux, T. N. Plasa, C. Busse and T. Michely, *New J. Phys.*, 2008, **10**, 043033.
33. Z. H. Ni, Y. Y. Wang, T. Yu, Y. M. You and Z. X. Shen, *Phys. Rev. B*, 2008, **77**, 235403.
34. R. Q. Zhao, Y. F. Zhang, T. Gao, Y. B. Gao, N. Liu, L. Fu and Z. F. Liu, *Nano Res.*, 2011, **4**, 712-721.
35. X. S. Li, C. W. Magnuson, A. Venugopal, R. M. Tromp, J. B. Hannon, E. M. Vogel, L. Colombo and R. S. Ruoff, *J. Am. Chem. Soc.*, 2011, **133**, 2816-2819.
36. A. M. Horgan, *Surf. Sci.*, 1970, **23**, 259-282.
37. G. C. Allen, P. M. Tucker and R. K. Wild, *Oxid. Met.*, 1979, **13**, 223-236.
38. S. Nie, A. L. Walter, N. C. Bartelt, E. Starodub, A. Bostwick, E. Rotenberg and K. F. McCarty, *ACS Nano*, 2011, **5**, 2298-2306.
39. Q. Li, H. Chou, J.-H. Zhong, J.-Y. Liu, A. Dolocan, J. Zhang, Y. Zhou, R. S. Ruoff, S. Chen and W. W. Cai, *Nano Lett.*, 2013, online.
40. Y. Miyata, K. Kamon, K. Ohashi, R. Kitaura, M. Yoshimura and H. Shinohara, *Appl. Phys. Lett.*, 2010, **96**, 263105.